

# The antiferromagnetic insulator $\text{Ca}_3\text{FeRhO}_6$ : characterization and electronic structure calculations

Volker Eyert and Udo Schwingenschlögl

*TP II, Institut für Physik, Universität Augsburg, D-86135 Augsburg, Germany*

Raymond Frésard, Antoine Maignan, Christine Martin, and Ninh Nguyen

*Laboratoire CRISMAT UMR CNRS-ENSICAEN 6508,  
6 Boulevard Maréchal Juin, 14050 Caen Cedex, France*

Christian Hackenberger and Thilo Kopp

*EP VI, Center for Electronic Correlations and Magnetism,  
Institut für Physik, Universität Augsburg, D-86135 Augsburg, Germany*  
(Dated: November 2, 2018)

We investigate the antiferromagnetic insulating nature of  $\text{Ca}_3\text{FeRhO}_6$  both experimentally and theoretically. Susceptibility measurements reveal a Néel temperature  $T_N \simeq 20$  K, and a magnetic moment of  $5.3\mu_B/\text{f. u.}$ , while Mössbauer spectroscopy strongly suggests that the Fe ions, located in trigonal prismatic sites, are in a  $3+$  high spin state. Transport measurements display a simple Arrhenius law, with an activation energy of  $\sim 0.2$  eV. The experimental results are interpreted with LSDA band structure calculations, which confirm the  $\text{Fe}^{3+}$  state, the high-spin/low-spin scenario, the antiferromagnetic ordering, and the value for the activation energy.

PACS numbers: 71.20.-b, 75.25.+z, 75.10.Pq, 75.50.Ee

Keywords: electronic structure, low-dimensional antiferromagnets, magnetic chains.

## I. INTRODUCTION

Interest in transition metal oxides has never been restricted to the most spectacular phenomenon of the high- $T_c$  superconductivity, but also concerns, *inter alia*, metal-insulator transitions, colossal magnetoresistance, and magnetic and orbital ordering [1]. Among the numerous magnetic transitions that have been studied, most of them are associated with structural transitions [2]. In contrast, no anomalous temperature dependence of the structural parameters has been reported in the  $m = 0$ ,  $n = 1$  members of the oxides family  $\text{A}_{3n+3m}\text{A}'\text{B}_{3m+n}\text{O}_{9m+6n}$ , which are currently attracting much attention [3]. These  $\text{A}_3\text{A}'\text{BO}_6$  compounds crystallize in the  $\text{K}_4\text{CdCl}_6$  structure which consists of infinite chains along the  $c$ -axis made of a  $1 : 1$  alternation of face-shared trigonal prisms  $(\text{A}'\text{O}_6)_{\text{TP}}$  and octahedra  $(\text{BO}_6)_{\text{Oct}}$ . According to their rhombohedral symmetry, the A cations separate the chains, the latter forming a hexagonal array. For such compounds, when the A' trigonal prism (TP) site is occupied by a magnetic cation, this provides interesting physical properties created by the co-existence of one-dimensionality character and geometrical frustration. This is illustrated by  $\text{Ca}_3\text{Co}_2\text{O}_6$  for which the ordered antiferromagnetic state below  $T_N \sim 26$  K [4, 5] bears some similarity to the partially disordered antiferromagnetic (PDA) state as originally proposed for  $\text{ABX}_3$  geometrically frustrated 1D compounds [6]. But in marked contrast with the  $\text{ABX}_3$  members, the intra-chain coupling in  $\text{Ca}_3\text{Co}_2\text{O}_6$  is ferromagnetic [4] and the magnetic field induced magnetization is very spectacular [7, 8, 9, 10]. Indeed, as a function of the applied magnetic field, several magnetization jumps with a constant

field spacing are observed. Besides, the saturation magnetization is larger than expected from the assumption of different spin states for  $\text{Co}^{3+}$  high spin (HS) and low spin (LS) in the TP and oct., respectively. Nonetheless, the ferromagnetic coupling along the chains is probably related to this “spin state ordering”, the latter resulting from the different crystalline electrical fields in each  $\text{Co}^{3+}$  polyhedron. Such a coupling is likely to involve both LS  $\text{Co}^{3+}$  and O ions [11, 12, 13]. In that respect, the different magnetic behavior of the two isostructural compounds  $\text{Ca}_3\text{FeRhO}_6$  and  $\text{Ca}_3\text{CoRhO}_6$  is worth mentioning [14, 15, 16, 17, 18, 19, 20, 21]. In the latter, the ferromagnetic intrachain coupling is expected as  $\text{Rh}^{3+}$  is isoelectronic to  $\text{Co}^{3+}$  ( $3d^6$ ), whereas the global magnetic behavior of  $\text{Ca}_3\text{FeRhO}_6$  appears to be antiferromagnetic although  $\text{Fe}^{3+}$  ( $d^5$ ) or  $\text{Fe}^{2+}$  ( $d^6$ ) are both HS cations with large  $S$  values ( $5/2$  or  $2$ ). Such different background states for the  $\text{Ca}_3\text{MRhO}_6$  1D compounds (with  $\text{M} = \text{Fe}$  and  $\text{M} = \text{Co}$ ) suggest subtle changes of the electronic structure.

In  $\text{Ca}_3\text{FeRhO}_6$ , contradicting results have been reported for the oxidation states of iron and rhodium cations which add more complexity to the interpretation. In order to shed light on the magnetic and electronic behavior of  $\text{Ca}_3\text{FeRhO}_6$ , we compare, in continuation of previous work [22], results of band structure calculations to the electrical and magnetic properties, together with Mössbauer spectroscopy measurements.

## II. EXPERIMENTS

The polycrystalline sample of  $\text{Ca}_3\text{FeRhO}_6$  was prepared by mixing the precursors  $\text{CaO}$ ,  $\text{Fe}_2\text{O}_3$  and  $\text{Rh}_2\text{O}_3$  in the molar ratios 3 : 0.5 : 0.5. The thoroughly mixed powder, pressed in bars ( $\sim 2 \times 2 \times 10 \text{ mm}^3$ ) was first heated at  $900^\circ\text{C}$  for 24h and then at  $1250^\circ\text{C}$  for a  $3 \times 24 \text{ h}$  period with intermediate X-ray controls. The crystallinity and purity of the obtained black product were checked by X-ray powder diffraction. The diffraction peaks have been indexed in the space group  $R\bar{3}c$  with  $a$  and  $c$  values very close to those reported in Refs. [14, 15], allowing to refine the 3 : 1 : 1 ratio for the cation  $\text{Ca} : \text{Fe} : \text{Rh}$  with an uncertainty of approximately 3 % which is acceptable in all respects. Besides, small intensity peaks were also found, that could be attributed to  $\text{Ca}_2\text{Fe}_2\text{O}_5$ . Magnetic measurements were performed with a SQUID magnetometer. Electrical resistivity was measured by the four probe technique. The four electrical contacts were ultrasonically deposited on a bar. The measurements were made by using a physical properties measurement system (PPMS). The  $^{57}\text{Fe}$  powder Mössbauer resonance spectrum at room temperature was performed with a transmission geometry by use of a constant acceleration spectrometer and a  $\gamma$ -ray source from  $^{57}\text{Co}$  embedded in a rhodium matrix. The velocity scale was calibrated with an  $\alpha$ -Fe foil at room temperature. The spectra were fitted with Lorentzian lines by the unpublished MOSFIT program. The isomer shift was referred to metallic  $\alpha$ -Fe at 293 K.

## III. RESULTS

### A. Magnetism

When compared to the  $T$ -dependent reciprocal magnetic susceptibility curve [ $\chi^{-1}(T)$ ] of  $\text{Ca}_3\text{Co}_2\text{O}_6$  as given in Ref. [9], the  $\chi^{-1}(T)$  curve of  $\text{Ca}_3\text{FeRhO}_6$  (Fig. 1) exhibits a much more linear behavior extending over a larger  $T$  range. This result reflects a lack of ferromagnetic interactions for the latter as also attested by the different extrapolated temperatures for  $\chi^{-1}(T = \theta_{\text{CW}}) = 0$ , the Curie-Weiss temperature  $\theta_{\text{CW}}$  values being  $-20 \text{ K}$  and  $+25 \text{ K}$  for  $\text{Ca}_3\text{FeRhO}_6$  and  $\text{Ca}_3\text{Co}_2\text{O}_6$ , respectively. Furthermore in  $\text{Ca}_3\text{Co}_2\text{O}_6$ , a  $\chi^{-1}$  drop below  $T_N \sim 26 \text{ K}$  is observed, which indicates that a net ferrimagnetic state is reached: on each triangle made by three neighboring  $\text{CoO}_6$  chains, two chains are antiferromagnetically coupled (zero net magnetic moment) whereas the third one exhibits a net ferromagnetic magnetization along the direction of the external applied magnetic field. In contrast, the  $\chi^{-1}(T)$  curve of  $\text{Ca}_3\text{FeRhO}_6$  exhibits a  $\chi^{-1}$  increase below  $\sim 20 \text{ K}$  indicative of a 3D antiferromagnetic phase. Analysis of the slope along the linear region yields an effective paramagnetic moment  $\mu_{\text{eff}}(\text{exp.}) = 5.3\mu_B/(\text{Fe} + \text{Rh})$ . We will refer to this experimental value below in subsection C.

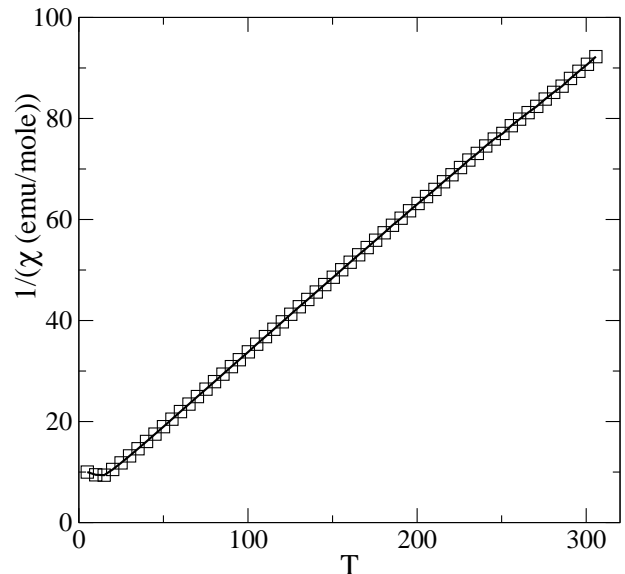


FIG. 1: Susceptibility of  $\text{Ca}_3\text{FeRhO}_6$ .

The RT Mössbauer spectrum of this compound consists of a paramagnetic doublet and is consistent with the measurements reported in Ref. [16]. However, the best fit was obtained with two Mössbauer components, the hyperfine parameters of which are given in Table I. The observed isomer shift value ( $IS = 0.45 \pm 0.1 \text{ mm/s}$ ) of the main component ( $\% = 96 \pm 2$ ) is typical of  $\text{Fe}^{3+}$  ions. Its high absolute quadrupole splitting value ( $QS = 1.20 \text{ mm/s}$ ) shows that this site is not in the octahedral symmetry, and therefore the Fe ions are located in trigonal sites. For the minor Mössbauer component ( $\% = 4 \pm 2$ ), the IS value of  $0.73 \pm 0.1 \text{ mm/s}$  is rather corresponding to  $\text{Fe}^{2+}$  ions. Therefore the vast majority of iron ions in  $\text{Ca}_3\text{FeRhO}_6$  are in the trivalent state.

### B. Transport

The second set of measurements concerns the expected localized nature of the electrical transport. Indeed, as shown in Table II,  $\text{Ca}_3\text{FeRhO}_6$  appears far more insulating than the related Co compounds since, for instance at 300 K, the resistivity  $\rho$  for  $\text{Ca}_3\text{FeRhO}_6$  is 160 times larger than that of  $\text{Ca}_3\text{Co}_2\text{O}_6$  [23]. The  $T$ -dependence of the resistivity confirms that  $\text{Ca}_3\text{FeRhO}_6$  is insulating, as

TABLE I: Refined  $^{57}\text{Fe}$  Mössbauer hyperfine parameters of  $\text{Ca}_3\text{FeRhO}_6$  at room temperature including the linewidth  $\Sigma$ , and % : relative intensity of the Mössbauer site.

IS (mm/s)	$\Sigma$ (mm/s)	QS (mm/s)	%
0.45 (1)	0.28 (1)	1.20 (1)	96 (2)
0.73 (1)	0.36 (1)	1.49 (1)	4 (2)

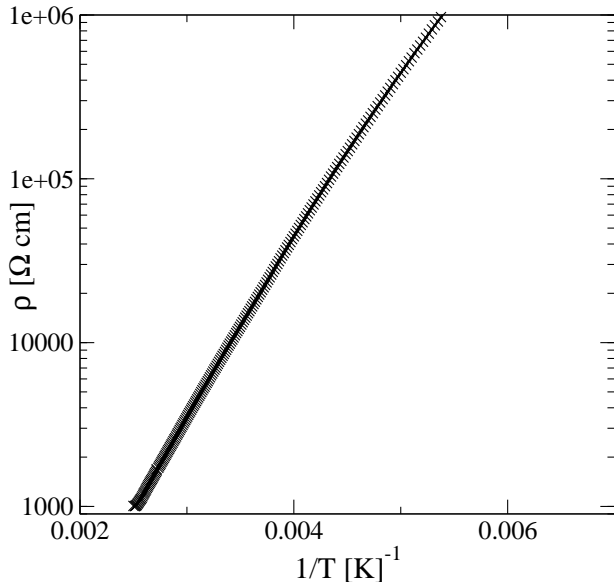


FIG. 2: Temperature dependence of the resistivity of  $\text{Ca}_3\text{FeRhO}_6$ , yielding an activation temperature  $T_0 = 2200\text{K}$ .

shown in Fig. 2. As  $T$  decreases,  $\rho$  increases very rapidly in  $\text{Ca}_3\text{FeRhO}_6$  reaching the set-up limit (corresponding to  $\sim 10^6\Omega$ ) at  $\sim 230\text{K}$ . For the available  $T$ -range, the linear  $\ln \rho (T^{-1})$  curve shows that a simple Arrhenius law is followed from which an activation energy of  $0.2\text{eV}$  can be extracted. According to both, high  $\rho$  value and thermally activated behavior, it turns out that in  $\text{Ca}_3\text{FeRhO}_6$ , the charge carriers are localized. Such a result is consistent with the antiferromagnetic intrachain coupling. These data for  $\text{Ca}_3\text{FeRhO}_6$  confirm that despite the existing similarities to isostructural  $\text{Ca}_3\text{CoRhO}_6$ , i.e., the  $\text{A}'_{\text{TP}}$  and  $\text{B}_{\text{oct}}$  crystallographic sites are also occupied by trivalent cations with high spin ( $S=5/2$  for  $\text{Fe}^{3+}$ ) and low spin ( $S=0$  for  $\text{Rh}^{3+}$ ), respectively, the nature of the magnetic interactions differs strongly.

### C. Band structure calculations

For the LSDA band structure calculations we used the augmented spherical wave (ASW) method in its scalar-relativistic implementation [24, 25]. In the ASW method, the wave function is expanded in atom-centered augmented spherical waves, which are Hankel functions

TABLE II: Comparison of the resistivities at room temperature.

compound	$\text{Ca}_3\text{Co}_2\text{O}_6$	$\text{Ca}_3\text{CoRhO}_6$	$\text{Ca}_3\text{FeRhO}_6$
$\rho(300\text{K}) [\Omega \cdot \text{cm}]$	50 [23]	39 [23]	8 300

and numerical solutions of Schrödinger's equation, respectively, outside and inside the so-called augmentation spheres. In order to optimize the basis set, additional augmented spherical waves were placed at carefully selected interstitial sites. The choice of these sites as well as the augmentation radii were automatically determined using the sphere-geometry optimization algorithm [26]. The Brillouin zone integrations were performed using the linear tetrahedron method with up to 85  $\mathbf{k}$ -points within the irreducible wedge. In contrast to our previous work [22] we here use a new version of the ASW code, which takes the non-spherical contributions to the charge density inside the atomic spheres into account.

All calculations are based on the powder data of Nitaka *et al.* [14]. In a first step, we performed a set of calculations, where spin-degeneracy was enforced. The resulting partial densities of states (DOS) are shown in Fig. 3. While O  $2p$  dominated bands are located in the

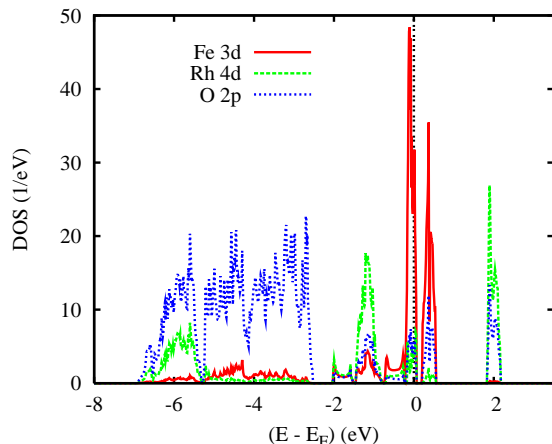


FIG. 3: (Color online) Partial densities of states (DOS) of spin degenerate  $\text{Ca}_3\text{FeRhO}_6$ .

interval from  $-6.8$  to  $-2.4\text{eV}$ , three groups of bands of mainly metal  $d$ -character are found at higher energies. However, the strong  $d$ - $p$  hybridization causes large  $p/d$  contributions above/below  $-2\text{eV}$ , reaching up to 50% especially for the Rh  $4d$  states.

According to the partial Fe  $3d$  densities of states shown in Fig. 4 the trigonal crystal field at the iron sites results in a splitting into non-degenerate  $d_{3z^2-r^2}$  as well as doubly degenerate  $d_{xy, x^2-y^2}$  and  $d_{xz, yz}$  states. The Rh  $4d$  states as given in Fig. 5 experience a nearly perfect separation of the  $4d$  states into occupied  $t_{2g}$  and empty  $e_g$  states due to the octahedral crystal field at these sites. Whereas strong  $\sigma$ -type  $d$ - $p$  bonding places the Rh  $4d$   $e_g$  states at  $2.0\text{eV}$ , the peak at about  $0.4\text{eV}$  traces back to Fe  $d_{xz, yz}$  states. For this reason, spin-polarization of the latter bands is highly favourable, with the observed high-spin/low-spin scenario.

In a second step, spin-polarized calculations were performed leading to the observed antiferromagnetic ordering, which is by  $1\text{mRyd}$  per Fe atom more stable than

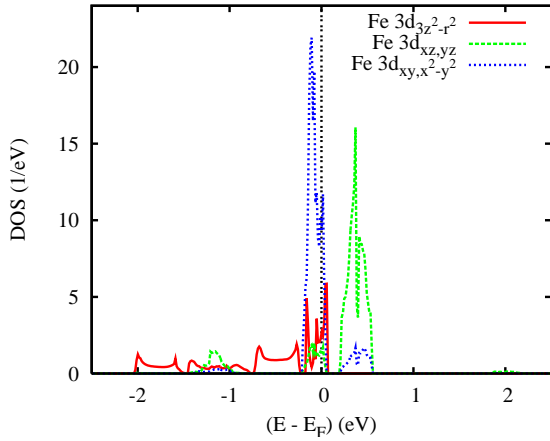


FIG. 4: (Color online) Partial Fe  $d$  DOS of spin degenerate  $\text{Ca}_3\text{FeRhO}_6$ .

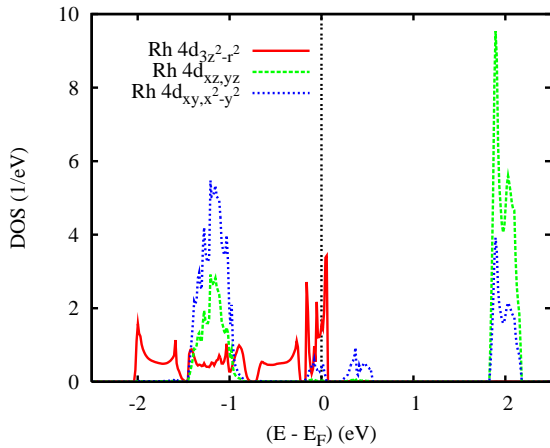


FIG. 5: (Color online) Partial Rh  $d$  DOS of spin degenerate  $\text{Ca}_3\text{FeRhO}_6$ .

the ferromagnetic configuration. Well localized magnetic moments of  $0.00 \mu_B$  (Rh),  $3.77 \mu_B$  (Fe),  $0.13 \mu_B$  (O), and  $0.01 \mu_B$  (Ca) are obtained in close agreement with those of previous calculations [27]. These values reflect the experimental result of low- and high-spin states at the octahedral and trigonal prismatic sites, respectively. The total moment per sublattice amounts to  $\pm 4.58 \mu_B$ , which still might be slightly altered by the inclusion of spin-orbit coupling, which is beyond the present work. In particular, the obtained total magnetic moment per sublattice is smaller than the experimental value deduced from Fig. 1 as was also observed for  $\text{Ca}_3\text{Co}_2\text{O}_6$  [12, 13].

Worth mentioning are the rather high magnetic moments at the oxygen sites arising from the strong  $d$ - $p$  hybridization, which sum up to about  $0.8 \mu_B$  per trigonal prism. Adding to the  $3d$  moment they lead to the for-

mation of extended localized moments already observed in  $\text{Ca}_3\text{Co}_2\text{O}_6$  [12] and confirm the formal Fe  $S = 5/2$  configuration, hence, the formal  $\text{Fe}^{3+}$  state. The high-spin behavior at the iron sites is clearly observed in the partial DOS shown in Fig. 6, where the Fe  $3d$  minority

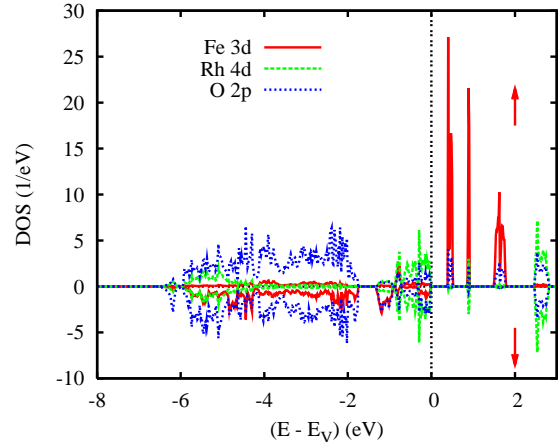


FIG. 6: (Color online) Partial DOS of antiferromagnetic  $\text{Ca}_3\text{FeRhO}_6$ .

states display sharp peaks above  $E_F$  and the spin majority states are spread over a large energy interval as a result of the strong  $p$ - $d$  hybridization.

The antiferromagnetic order growing out of the spin-polarized calculations goes along with the opening of an insulating gap of about 0.4 eV as revealed by Fig. 6. This value corresponds to an activation energy of 0.2 eV, which is in remarkably good agreement with the experimental value deduced from Fig. 2.

#### IV. SUMMARY

In summary, we have performed susceptibility, Mössbauer spectroscopy, and transport measurements on the antiferromagnetic insulating compound  $\text{Ca}_3\text{FeRhO}_6$ . The experimental data have been compared with LSDA band structure calculations, and the agreement is found to be very good. In particular, the calculations confirm several experimental key results as, e.g., the charge and spin states at the Fe and Rh sites including the characteristic high-spin/low-spin scenario, the antiferromagnetic ordering, and the activation energy.

#### V. ACKNOWLEDGEMENTS

This work is supported by the Deutsche Forschungsgemeinschaft through SFB 484.

[1] S. Maekawa, T. Tohyama, S. E. Barnes, S. Ishihara, W. Koshibae, and G. Khaliullin, *Physics of Transition*

*Metal Oxides*, (Springer Verlag, Berlin (2004)).

- [2] For a review, see *Colossal Magnetoresistance, Charge Ordering and Related Properties of Manganese Oxides*, edited by C. N. R. Rao and B. Raveau (World Scientific, Singapore, 1998) and *Colossal Magnetoresistance Oxides*, edited by Y. Tokura (Gordon & Breach, London, 1999).
- [3] K. E. Stitzer, J. Darriet, and H.-C. zur Loye, *Curr. Opin. Solid State Mater. Sci.* **5**, 535, (2001).
- [4] H. Fjellvåg, E. Gulbrandsen, S. Aasland, A. Olsen, and B. Hauback, *J. Solid State Chem.* **124**, 190 (1996).
- [5] S. Aasland, H. Fjellvåg, and B. Hauback, *Solid State Comm.* **101**, 187 (1997).
- [6] M. Mekata, *J. Phys. Soc. Jpn.* **42**, 76 (1977); M. Mekata and K. Adachi, *J. Phys. Soc. Jpn.* **44**, 806 (1978).
- [7] H. Kageyama, K. Yoshimura, K. Kosuge, H. Mitamura, and T. Goto, *J. Phys. Soc. Jpn.* **66**, 1607 (1997).
- [8] H. Kageyama, K. Yoshimura, K. Kosuge, M. Azuma, M. Takano, H. Mitamura, and T. Goto, *J. Phys. Soc. Jpn.* **66**, 3996 (1997).
- [9] A. Maignan, C. Michel, A.C. Masset, C. Martin, and B. Raveau, *Eur. Phys. J. B* **15**, 657 (2000).
- [10] A. Maignan, V. Hardy, S. Hébert, M. Drillon, M.R. Lees, O. Petrenko, D. McK. Paul, and D. Khomskii, *J. Mater. Chem.* **14**, 1231 (2004).
- [11] R. Frésard, C. Laschinger, T. Kopp, and V. Eyert, *Phys. Rev. B* **69**, 140405(R) (2004).
- [12] V. Eyert, C. Laschinger, T. Kopp, and R. Frésard, *Chem. Phys. Lett.* **385**, 249 (2004).
- [13] H. Wu, M.W. Haverkort, Z. Hu, D. Khomskii, and L. H. Tjeng, *Phys. Rev. Lett.* **95**, 186401 (2005).
- [14] S. Niitaka, H. Kageyama, M. Kato, K. Yoshimura and K. Kosuge, *J. of Solid State Chem.* **146**, 137, (1999).
- [15] M.J. Davis, M.D. Smith and H.C. zur Loye, *J. of Solid State Chem.* **173**, 122, (2003).
- [16] S. Niitaka, K. Yoshimura, K. Kosuge, K. Mibu, H. Mitamura, T. Goto, *J. of Magn. and Magn. Mater.* **260**, 48, (2003).
- [17] S. Niitaka, K. Yoshimura, K. Kosuge, M. Nishi, and K. Kakurai, *Phys. Rev. Lett.* **87**, 177202 (2001).
- [18] S. Niitaka, K. Yoshimura, K. Kosuge, A. Mitsuda, H. Mitamura, and T. Goto, *J. Phys. Chem. Solids* **63**, 999 (2002).
- [19] V. Hardy, M.R. Lees, A. Maignan, S. Hébert, D. Flahaut, and D. McK. Paul, *J. Phys. Condens. Matt.* **15**, 5737 (2003).
- [20] S. Niitaka, H. Kageyama, K. Yoshimura, K. Kosuge, S. Kawano, N. Aso, A. Mitsuda, H. Mitamura, and T. Goto, *J. Phys. Soc. Jpn.* **70**, 1222 (2001).
- [21] M. Loewenhaupt, W. Schäfer, A. Niazi, and E.V. Sampathkumaran, *Europhys. Lett.* **63**, 374 (2003).
- [22] V. Eyert, U. Schwingenschlögl, C. Hackenberger, T. Kopp, R. Frésard, and U. Eckern, *Prog. Solid State Chem.*, at press (arXiv:cond-mat/0509374).
- [23] A. Maignan, S. Hébert, C. Martin and D. Flahaut, *Mater. Sc. and Eng. B* **104**, 121 (2003).
- [24] A. R. Williams, J. Kübler, and C. D. Gelatt, Jr., *Phys. Rev. B* **19**, 6094 (1979).
- [25] V. Eyert, *Int. J. Quantum Chem.* **77**, 1007 (2000).
- [26] V. Eyert and K.-H. Höck, *Phys. Rev. B* **57**, 12727 (1998).
- [27] A. Villesuzanne and M.-H. Whangbo, *Inorg. Chem.* **44**, 6339 (2005).